Tellus (1990), *42B*, 100–117

Parameterization of vertical tracer transport due to deep cumulus convection in a global transport model and its evaluation with ^{222}Radon measurements

By J. FEICHTER* and P. J. CRUTZEN, *Max-Planck-Institute for Chemistry, P.O. Box 3060, D-6500 Mainz, FRG*

(Manuscript received 31 October 1988; in final form 2 August 1989)

ABSTRACT

A parameterization scheme is described for calculating upward transport of mass in precipitating convective cells. This scheme, which is largely based on the work of Austin and Houze is implemented in a global three-dimensional tropospheric chemistry model. The convective events are stochastically distributed in time and space. The vertical exchange of mass by the clouds is derived from the conservation of water given the convective amount of precipitation and average large-scale temperature and humidity distribution. The sensitivity of the scheme is tested by varying several key parameters in the model. The ensuing vertical transport of mass is presented and compared to other approaches. A further test was made with ^{222}Rn, a short-lived radioisotope which is largely released from land surfaces. The simulated distribution is in good agreement with measurements. The importance of convective processes for the transport of short-lived tracers is clearly demonstrated.

1. Introduction

A global 3-dimensional model has been developed to simulate the transport and chemistry of important tracer constituents in the troposphere. The purpose of the model is to determine the climatology of chemical tracers rather than to simulate episodic events. Tracer transport in the model is based on monthly means of observed wind fields from 1963 to 1973 by Oort (1983). Simulation runs with F11 and F12 (Zimmermann, 1984; Zimmermann, 1987) and with the radioactive tracer ^{85}Kr (Zimmermann et al., 1989) were performed to test the transport scheme. However, in order to achieve a realistic spatial distribution of the trace substances it is necessary to consider the effects of subgrid scale processes. For short-lived tracers, vertical transport from the boundary layer to the middle and upper troposphere, by deep cumulus convection is of particular importance.

In the updrafts of convective cells, tracers are transported rapidly from the ground to the upper troposphere, often within about one hour. Thus considerable vertical mixing occurs during isolated events of great rapidity and depth. In comparison to the synoptic scale processes this vertical mixing takes place within such small time and space scales that the use of large scale vertical eddy diffusion coefficients makes it impossible for short-lived chemical tracers to reach the upper troposphere (Crutzen and Gidel, 1983). When averaging these processes, the implications of the strong vertical transport in clouds have traditionally not been considered in large scale photochemical models, although they were considered in a few studies (Chatfield and Crutzen, 1984; Gidel, 1983). Several global 3-dimensional models were developed during the last years but most of the general circulation models (GCM) used to obtain the input winds for the tracer model parameterized the convective

* Current address: University of Hamburg, Meteorological Institute, Bundesstraße 55, 2000 Hamburg 13, FRG.

processes with the "moist convective adjustment" (Mahlman and Moxim, 1978; Covey et al., 1985; Malone et al., 1986), which does not allow for movement of any quantity other than moist static energy. Prather et al. (1987) present a method to describe the vertical exchange of air by deep convection in a global 3-dimensional model. They saved the statistic of convective events over a period of hours H (1 month) as sampled by their GCM and assumed that each such event takes 50% of the mass in the bottom layer (k) to the top of the cloud (layer m). The average fraction of the mass in layer k which is convected to layer m during a 1-h time step over this averaging period H is calculated as $0.50\, n_{km}/H$, where n_{km} is the number of convective events. The fraction of the grid-box involved in convection during a time step of T hours in the transport model is then

$$c_{km} = 1 - (1 - 0.50\, n_{km}/H)^T.$$

This transport is balanced by subsidence within the same column of grid boxes.

As our model is driven by monthly climatological means, we have chosen another approach. We propose here a scheme, to a large degree based on an earlier GATE-study by Austin and Houze (1973). In our scheme, however, the effects of deep cumulus convection are implemented as stochastic processes. When a convective event takes place the upward transported air mass varies in time and space depending on the precipitation amount produced by convective clouds. This convective precipitation amount is derived by a climatology of the monthly precipitation and by the GCM-output (Dümenil and Schlese, 1987) of the percentage of large-scale and convective rain. In the following this scheme will be developed in some detail and tested, using ^{222}Rn as a tracer. ^{222}Rn is particularly suited for such studies as its sources are quite well known and its atmospheric lifetime is only determined by radioactive decay with a short half lifetime of 3.8 days.

2. The large scale transport model

The cumulus convection parameterization scheme, which will be presented in this paper, has been implemented in a global three-dimensional tracer transport model, the MOGUNTIA model, developed by Zimmermann (1984). The region of the Eulerian grid model covers the troposphere from 1000 hPa up to 100 hPa in 100 hPa layers except the lowest and the highest layers, which cover 50 hPa. The current version has a horizontal space resolution of 10° × 10° and uses two-hour time steps to integrate the continuity equation for the mixing ratio of chemical species in time:

$$\rho \frac{\partial \mu}{\partial t} = -\rho \boldsymbol{V} \nabla \mu - \nabla \rho (\boldsymbol{K} \nabla \mu) + Q, \qquad (1)$$

where

μ	mass mixing ratio of trace substance
ρ	air density in kg m^{-3}
t	time in s
$\boldsymbol{V}(u, v, w)$	three-dimensional wind vector in m s^{-1}
$\boldsymbol{K}(K_{xx}, K_{yy}, K_{zz})$	three-dimensional eddy diffusion tensor in m^2 s^{-1}
Q	source-sink term.

Mass-conserving three-dimensional wind fields are obtained from observed horizontal winds using an objective analysis procedure. Monthly wind fields are taken from the data-sets by Oort (1983) averaged over the period 1963–1973. The large scale diffusion coefficients are proportional to the day-to-day standard deviations of the monthly winds weighted with height dependent integral-time scales T (Murgatroyd, 1969; Kao, 1974).

$$K_{xx} = \overline{u'^2}\, T_u$$
$$K_{yy} = \overline{v'^2}\, T_v. \qquad (2)$$

T_u and T_v range from 5 to 25 h depending on height. Green (1970) gives a relationship between K_{yy} and K_{zz} through a particle displacement parameter α and an isentropic slope ε, according to

$$K_{zz} = \alpha^2 \varepsilon^2 K_{yy}. \qquad (3)$$

ε as a function of latitude and pressure is taken from Newell et al. (1972) and α, which is only height dependent, from Fig. 8 in Green (1970). The vertical component of the large-scale diffusivity in the lowest model layer above ground is interpolated from a profile by Smith (Pasquill, 1974) as a function of the large-scale temperature gradient near the ground. Smith's K values based on statistical properties of turbu-

lence are largely derived from measurements. Values over sea are taken to be four times lower than those over land (Delsol et al., 1971).

Exchange through the upper boundary at 100 hPa takes place only by diffusion along a prescribed, tracer dependent vertical concentration gradient.

Although daily wind- and temperature-fields are available we used monthly averaged means, because they allow very fast transport algorithm. It is therefore possible to prepare a transport-operator matrix for each month. To simulate the transport of one tracer over one year requires a computing time of 16 seconds on a CRAY-XMP. Thus the MOGUNTIA-model is an efficient transport model to investigate tropospheric chemistry. Model-runs with F11 and F12 (Zimmermann, 1984; Zimmermann, 1987) and ^{85}Kr (Zimmermann et al., 1989) show very good agreement with measurements.

3. The deep convection parameterization scheme

When implementing a scheme for calculating vertical convective fluxes in a transport model using climatological data-sets, three questions have to be answered:

1. When and where do convective events take place?
2. What is the vertical extension of the clouds?
3. What is the magnitude of vertical mass fluxes within the updraft of a single cell?

3.1. Distribution of convective events in time and space

Since the major part of convective mass transport occurs inside precipitating convective cells, as a first approximation, we concentrate our attention on transport in cumulonimbus (Cb) clouds. To obtain information about the frequency of Cb clouds, cloud atlases by Hahn et al. (1982) and by Warren et al. (1986) were consulted. These compile four seasonal data-sets describing the occurrence of Cb derived from ground based observations over an eleven year period. Frequency of occurrence in the atlas denotes the number of times Cb was reported to be present, divided by the number of synoptic reports inside a grid area. There statistics are used by the model in the following way: within each season the occurrence of Cb is distributed randomly among the days. The distribution of the occurrence of events during a single day is given by a probability function which takes into account that most convective events occur during the afternoon over land and during the morning over sea. For each grid-point the occurrence of convective events during the model simulation is determined by a random number generator without any consideration of correlations in time and space. Whenever a model convective event takes place a fraction of the boundary layer air in the entire grid-box is exchanged vertically with the rest of the atmosphere in the grid-box. The details of this procedure are explained in the following text.

3.2. Distribution of cloud heights within a cloud cluster

The vertical transport of the mass of air inside the updraft of a convective cell (or cloud) is computed according to Austin and Houze (1973). The method is based on a relation between the water content and the upward flux of humid air masses inside a convective cell. The water content of a convective cell is determined by the amount of precipitation. Therefore the parameterization of the convective mass fluxes is assumed to be a function of the convective precipitation and of the large-scale temperature and humidity. Since convective events consist of clouds of varying depths, constituting so-called cloud clusters, this method requires statistical information about the cloud height distribution within such clusters.

The cloud base is assumed always to be located at the 900 hPa level. At all latitudes the convective cloud tops are presumed to reach at least the 700 hPa level. Smaller cumuli inside such a convective cloud cluster are not considered since they do not significantly contribute to precipitation and to vertical mass fluxes. Ruprecht (1982), who calculated cloud mass fluxes of tropical cloud clusters, found the contribution of shallow clouds to be less than 1% of that resulting from deep convection. Maximum cloud top levels depend on the latitude and are 100 hPa between 0 and 25°, 200 hPa between 25 and 55° and 300 hPa at latitudes higher than 55°. Not all clouds, however, reach this maximum

Table 1. *Percentage contribution to the total convective precipitation amount produced by ensembles of clouds with varying cloud top levels for given maximum cloud top heights*

Max. cloud top	Cloud top [hPa]						
[hPa]	100	200	300	400	500	600	700
100	28	24	21	11	9	4	3
200		32	27	20	12	5	4
300			38	31	17	9	5

altitude. Instead, the vertical extent of the clouds are assumed to be distributed in 100 hPa steps between the 700 hPa level and the maximum cloud top level, in accordance with the model resolution. The fraction of total precipitation produced by individual cells as a function of their depth was taken from Cheng and Houze (1979) (as interpreted by Frank and Cohen, 1985). Their fractions, which are based on radar echo observations in the GATE program, are summarized in Table 1. We thus characterize the fraction of clouds reaching a certain height through their relative contribution to the total precipitation. Data solely derived from studies in parts of the tropics applied to a global model are only useful in a first approach and it is clearly necessary to get a better global distribution of cloud heights.

3.3. *Computation of vertical transport*

To calculate the vertical transport of air masses inside a single cloud type, defined by its vertical extension, we consider the effects of lifting, entrainment and detrainment over the life-cycle of the cloud in terms of the conservation of water vapor in a grid box bounded by the levels z and dz as shown in Fig. 1 (Austin and Houze, 1973).

The mass balance equation for water vapor is

$$M_U q_U - (M_U + dM^e - dM^d)(q_U + dq_U) - dM^d(q_U + 0.5\,dq_U) + dM^e(q_E + 0.5\,dq_E) = dC \quad (4)$$

with the following symbols:

M_U mass of air which rises vertically through level z
dM^e mass of air entrained into the updraft
dM^d mass of air detrained into the environment
q_U mixing ratio of water vapor in updraft
q_E mixing ratio of water vapor in environment
dC amount of water condensing in the layer $z, z + dz$.

Neglecting products of differentials and defining the entrainment rate,

$$E = \frac{1}{M_U}\frac{dM^e}{dz}, \quad (5)$$

eq. (4) can be rewritten:

$$dC = M_U\left[E(q_E - q_U) - \frac{dq_U}{dz}\right]dz. \quad (6)$$

Integrating eq. (6) through the depth of the cloud we get a relation between the total condensate C integrated over the life-time of the cloud and the upward mass transport $M_U(z)$ throughout the cloud

$$C = \int_{z_{base}}^{z_{top}} M_U\left[E(q_E - q_U) - \frac{dq_U}{dz}\right]dz. \quad (7)$$

To solve eq. (7) for $M_U(z)$, we adopt a particular shape function for M_U, such that

$$M_U(z) = M_U(\zeta) f(z), \quad (8)$$

where ζ is the level of maximum upward flux, which, based on observations, may be approximated from the expression

$$\zeta = z_{base} + \alpha(z_{top} - z_{base}). \quad (9)$$

α ranges from 0.75 in the tropics to 0.5 in mid-latitudes. Following Austin and Houze (1973) the

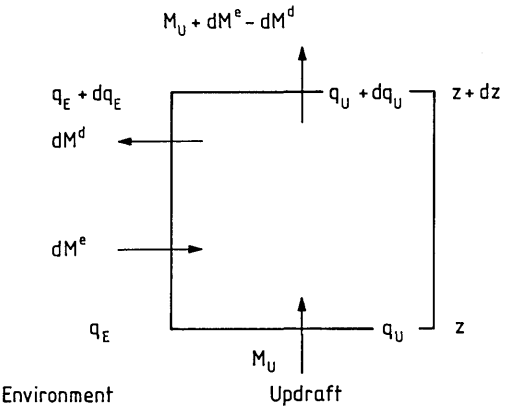

Fig. 1. Mass balance diagram of water vapor in a box bounded by the levels z and dz.

shape function $f(z)$ is taken as

$$f(z) = \frac{2}{2-E}\exp(E(z-\zeta)) - \frac{2}{2-E}\exp(2(z-\zeta)) \quad (10)$$

between $z = z_{base}$ and $z = \zeta$. The function $f(z)$ increases with height until $z = \zeta$ as would be expected for a cell of constant entrainment rate. Above ζ, $f(z)$ decreases parabolically $\left(f(z) = \left(\frac{z_{top} - z}{z_{top} - \zeta}\right)^2\right)$ to zero at the top of the cloud.

$M_U(\zeta)$ is derived from eq. (7) and eq. (8) as

$$M_U(\zeta) = C \Big/ \int_{z_{base}}^{z_{top}} f(z)\left[E(q_E - q_U) - \frac{dq_U}{dz}\right] dz. \quad (11)$$

To solve eq. (11) for $M_U(\zeta)$, based on observations, several approximations are adopted (Austin and Houze, 1973):

(1) The entrainment rate is assumed to be constant with altitude

$$E = \frac{a}{0.13(z_{top} - z_{base} - 1)}\,[\mathrm{km}^{-1}]. \quad (12)$$

Eq. (12) indicates an inverse relation between entrainment rate and cell height with the value of E covering the range 1.0 to 0.1 km^{-1} for cells varying in depth between 2.5 and 16.0 km for $a = 0.2$ (Austin and Houze, 1973).

(2) The environmental values T_E are taken the Oort data set. To a first approximation it is assumed that the entrained air is saturated. This follows the procedure of Austin and Houze (1973), who considered, however, a mesoscale system and not such large scale grid-boxes as we have adopted in this study.

(3) Assuming saturation inside the cloud, $q_U(z)$ depends only on $T_U(z)$ at each level. We use a similar buoyancy equation as described by Austin and Houze (1973) to calculate the temperature excess $T_U - T_E$, which gives us $T_U(z)$.

$$w_U(z)\frac{dw_U(z)}{dz} = -w_U^2(z)E + g\left(\frac{T_U^v - T_E^v}{T_U^v}\right), \quad (13)$$

where the superscript v means the virtual temperature and T_E is set to be the large-scale temperature. To solve this equation the vertical velocity inside the updraft is postulated with the same profile as $M_U(z)$, i.e.,

$$w_U(z) = w_{max} f(z). \quad (14)$$

Values of w_{max} for cells of different depths from 2–14 km are based on measurements and range from 3–9 m s^{-1} (see Table 2).

(4) The total amount of condensed water C that is formed during the life-cycle of a convective cell is assumed to be three times the precipitation, corresponding to a precipitation efficiency of 33%. This value was given by Austin and Houze (1973) as an average based on several observations indicating values from 10–50%. We have done radon simulations assuming a higher precipitation efficiency over sea, but the differences are negligible as radon is emitted only from land surfaces.

The precipitation at each grid point per convective event during a particular month is taken as

$$P_c = P * F_c * F_d / N_c \quad (15)$$

with the following symbols:

- P monthly mean of precipitation by a climatology of Jaeger (1976)
- F_c fraction of convective rain taken from the ECMWF model (Dümenil and Schlese, 1987)
- F_d fraction of convective rain caused by clouds with given depth
- N_c number of convective events per month.

With these assumptions, through eqs. (8) and (11) it is possible to compute the function $M_U(z)$ for clouds with a given cloud depth. Finally, the fractional contributions of the mass transport by clouds with various depths $M_U(z)_i$ are added together to give the total upward transported mass of air inside a grid box during a model convective event

$$M_U(z) = \sum_i M_U(z)_i. \quad (16)$$

Table 2. *Vertical velocities for model cells at the level of maximum updraft after Austin and Houze (1973)*

Cell depth (km)	1–3	3–5	5–7	7–9	9–11	11–13	13–15
w_{max} (m s^{-1})	3	4	5	6	7	8	9

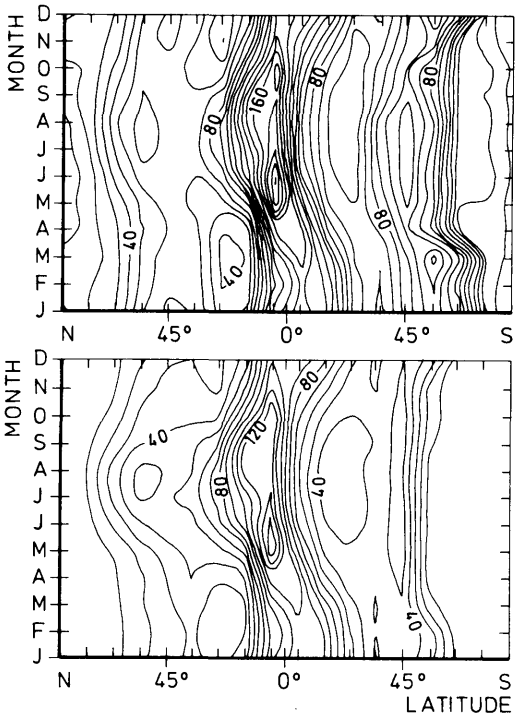

Fig. 2. Latitudinal and seasonal distribution of the zonally averaged amount of precipitation; upper graph: Total amount of precipitation by Jaeger (1976) in mm per month; lower graph: Convective precipitation amount in mm per month.

The zonally averaged monthly amount of precipitation and the convective precipitation are shown in Fig. 2. The convective activity is distinctly marked in northern mid-latitudes during summer months, while most precipitation at high- and mid-latitudes in the southern hemisphere is produced by large-scale processes. In the tropics convective activity exceeds large-scale precipitation all year.

The number of convective events reflects the same seasonal and geographical distribution. Fig. 3 shows the zonally average number of events per month as derived from the NCAR cloud atlas. Highest convective activity with a maximum of almost one event per day is found within the ITCZ during summer and fall. South of 65°S no convective event takes place for the whole year.

The distribution of convective events for each time step and the vertical profiles of mass fluxes

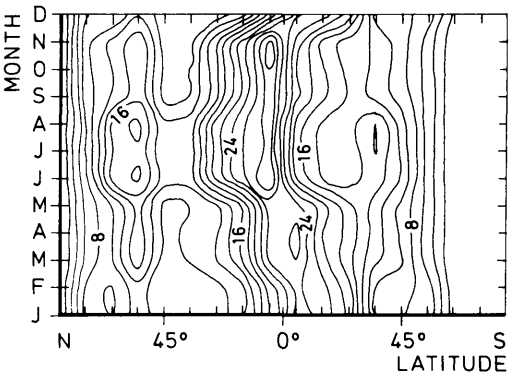

Fig. 3. Latitudinal and seasonal distribution of the zonally averaged number of events per month.

for each month are calculated and stored before the large scale transport model is started. During the model performance at each grid point and at each time-step a check is made if a convective event takes place. In case of a convective event air mass is transported from the lower levels to the upper troposphere which results in a redistribution of tracer concentration within a model grid-box. The redistribution is executed in three steps:

1. In the lower levels air mass is drawn into the updrafts and transported to higher levels. Within the updrafts the air mass becomes well mixed and is then detrained in the upper troposphere. Hence, gain or loss of air mass in each level is determined by $\Delta_z M_U(z)$.

2. After each convective event, at each pressure level, a new distribution of tracers is determined by a weighted average between the original tracer distribution and the vertically exchanged air. This method assumes, that horizontal exchange in a grid-box is rapid enough to level out concentration differences between the cloud area and its environment within the time step of two hours.

3. Subsidence in the environment outside the cloud area maintains the large scale mass balance.

4. Calculated mass transports

Fig. 4 depicts the vertical distribution of the calculated, zonally averaged upward transported air mass per grid-point and month. Strongest

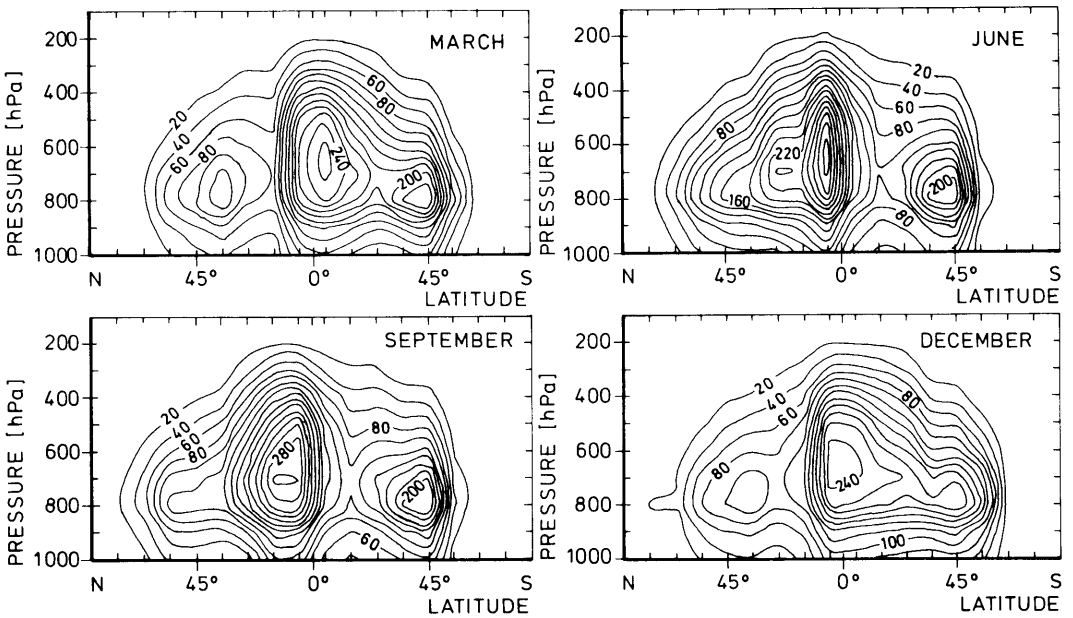

Fig. 4. Vertical and latitudinal distribution of the zonally averaged, vertically transported air mass per grid-box (10° × 10°) and month in units of 10^{17} *g*.

upward transport occurs, as one would expect, in the tropics during June between 700–600 hPa with a magnitude of 3×10^{19} g per month and grid-box. In the tropics this implies a complete mass exchange of the lowest 2 km layer within two to four days. The mass exchange decreases towards higher latitudes and vanishes in the polar regions. In mid-latitudes we find maximum values in the summer hemisphere.

To test our deep convection scheme we used results by Braham (1952), who estimated the mass transport in convective cells. He derived the total mass influx into the cloud from the horizontal velocity convergence and checked whether the water content of the inflow and the released latent heat were sufficient to provide for all the water sinks and to do the work implied by the vertical mass exchange. Based on observations of 53 summer time convective cells during the "Thunderstorm Project" in Ohio/USA he found a mean total amount of precipitation of 1.24×10^{11} *g* for an average thunderstorm cell. The average vertical mass exchange estimated by Braham inside the observed updrafts reaching up to 300 hPa is given in Fig. 5 (curve A) and is compared to our model results depicted as curves

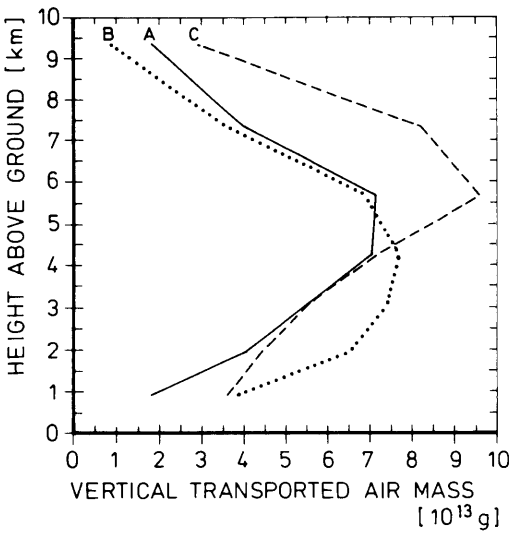

Fig. 5. Vertical profile of the vertically transported air mass in units of 10^{13} *g* inside a cell producing a precipitation amount of 1.24×10^{11} *g*. (A) Estimation of Braham (1952). (B) Model results for a cloud cluster consisting of cells varying in depth between 700 hPa and 300 hPa. (C) Model results assuming all clouds have their tops at 300 hPa.

B and C. Curve B shows the mass exchange of a cloud ensemble consisting of clouds with cloud tops ranging from 700 hPa to 300 hPa. The amount of 1.24×10^{11} g of rainfall is distributed among the various cloud depths according to Table 1. Curve C shows the vertically exchanged masses if we would assume that all clouds would have their top at 300 hPa and produce the same amount of precipitation as Braham's average convective cell.

Taking into account that the model uses mean climatological values of T_E and that most of the parameters of our scheme are derived from measurements of tropical cloud clusters, the profiles agree surprisingly well and indicate that our scheme may also be applicable to other latitudes, especially to simulate summer time convection.

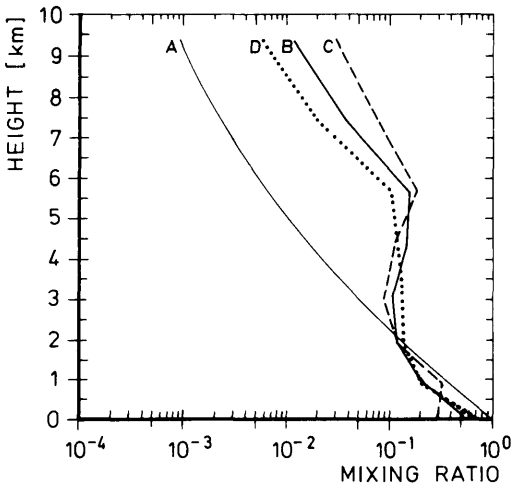

Fig. 6. Vertical profiles of the redistribution of the mass mixing-ratios of a tracer for different cloud height distributions, following a single convective event. A denotes the initial tracer profile, B the redistribution of the tracer using the cloud height distribution in Table 1, C the redistribution by a single cloud reaching up to 300 hPa, and D for the case that all clouds contribute equally to the precipitation.

5. Sensitivity tests of the convective scheme

Some assumptions in our scheme are rather arbitrary. Therefore, we try to estimate the influence of different choices of model parameters on calculated tracer concentration distributions. Test runs were made using an initial vertical tracer distribution which decreases exponentially with height. To demonstrate the influence of different assumptions this inert tracer is transported in a 1-dimensional box by convective processes only over a two-hour time step. To calculate the upward mass transports we use a precipitation amount of 7×10^{15} g during a convective event over a grid box, which is a good order of magnitude approximation for summertime continental mid-latitude conditions. We set the maximum cloud top level at 300 hPa and adopt a representative vertical temperature profile from the Oort data set, corresponding to that of Ohio during summer time. The following sensitivity analyses were conducted.

(1) As the percentage of precipitation produced by clouds reaching different heights taken from Cheng and Houze (1979) in the tropics, but adopted at other latitudes as well due to the lack of global convective cloud-height distributions, uncertainties are introduced, which we address by comparing computational results making two following assumptions. In the first one (curve C in Fig. 6), all preciptiation is produced by clouds with cloud tops at 300 hPa; in the second one, all clouds with cloud tops ranging between 700 and 300 hPa are assumed to make the same contribution to the precipitation amount (curve D in Fig. 6). Results are compared with the cloud distribution as described in Subsection 3.2 (curve B). Curve A in Fig. 6 denotes the initial tracer distribution. Although the assumptions made in C and D are rather different, the calculated mixing-ratios do not differ by more than a factor of about two from those in case B.

(2) The magnitude of the upward transported air mass inside a single cell depends strongly on the amount of water which condenses in convective clouds. To derive this amount from precipitation data Austin and Houze (1973) estimated an average precipitation efficiency of 33%, based on a literature survey indicating values mostly ranging from 10–50%. This has also been our basic assumption. However, Houze and Leary (1976) found a precipitation efficiency of 74% in tropical maritime clouds, which may precipitate more efficiently than continental clouds or thunderstorms at mid-latitudes. For storms in Ohio, USA, Braham (1952) calculated that 19% of the condensate reached the ground as precipitation. Based on these data we, therefore,

varied the precipitation efficiency in our scheme between 20 and 80%. Vertical profiles of the calculated redistribution of mixing-ratios following one convective event are shown in Fig. 7. Curve A denotes again the initial tracer profile. The vertical exchange is stronger when the precipitation efficiency is lower and vice versa. The mixing-ratios calculated with a precipitation efficiency of 80% (curve B) above 800 hPa are up to a factor of about three lower at 100 hPa compared to that calculated with a 33% precipitation efficiency (curve C). The mixing-ratios using a precipitation efficiency of 20% shown by curve D exceed those of curve C in all levels above 900 hPa; whereas, the surface mixing-ratio is lower by a factor of 20. Since a precipitation efficiency of 80% is quite high and the differences between cases B and C are relatively small, the precipitation efficiency of 33% by Austin and Houze (1973) for the entire model area seems to be a good compromise.

(3) To calculate the mass transport, a vertical profile of M_U and w_U is prescribed. The profile used in the model shows minima at the base and at the top of the cloud and a maximum at the height ζ. Braham's (1952) analysis of the "Thunderstorm Project" in Ohio indicates a maximum approximately halfway between cell base and top. Based on data from studies in the tropics, Austin and Houze (1973) stated that the net outflow is located in the upper 1/3 to 1/2 of the cells, while one-dimensional models suggest a maximum mass transport at the cell top with the outflow occurring in a thin layer. In our simulation, cell center and cell top are assumed as limits for the position of ζ. Fig. 8 depicts the redistribution of a tracer when in formula (9) α is set equal to 0.5 (case B) and to 0.75 (case C). Case C yields higher mass exchange near the surface and higher mixing-ratios in the upper atmosphere, but differences are quite small. When we assume cloud top as the level of maximum mass transport, the vertical exchange at the surface is more than one order of magnitude larger than the mass of the lowest grid-box.

(4) The vertical mass transport profile depends also on the entrainment rate. Studies showed that realistic thunderstorms cannot develop with entrainment rates larger than 0.5 km^{-1} (Austin and Houze, 1973). Therefore, setting $a = 0.2$ in formula (12) clouds with a depth larger than 2 km respectively a cloud top higher than 800 hPa can contribute to convective precipitation as we have

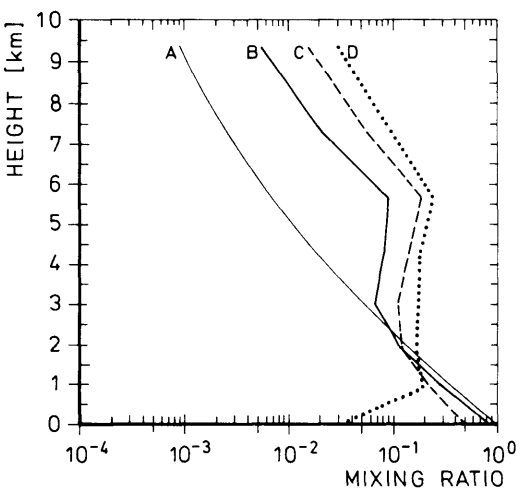

Fig. 7. Vertical profiles of the redistribution of the mass mixing-ratios of a tracer for varying precipitation efficiencies E, following a single convective event. Curve A shows the initial tracer distribution, B the redistribution by convective transport with $E = 80\%$, C with $E = 33\%$ and D with $E = 20\%$.

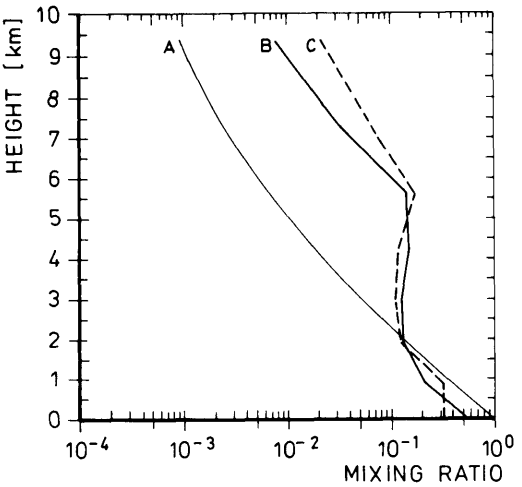

Fig. 8. Vertical profiles of the redistribution of the mass mixing-ratios of a tracer for varying levels of maximum updraft ζ, following a single convective event. Curve A shows the initial tracer distribution, B the redistribution by convective transport with $\alpha = 0.5$ and C with $\alpha = 0.75$ (see formula (10)).

assumed in our scheme (see Table 1). Assuming $a = 0.5$ enables only clouds reaching higher than 300 hPa a sufficient development. Thus a reasonable range for values of the entrainment rate are $a = 0.5$ in formula (12) (curve D), the standard case with $a = 0.2$ (case C) and $a = 0$ as lower limit. The variation of the entrainment rate influences not only the shape function $f(z)$ through eq. (10) but also the calculated values of the humidity inside the cloud q_U. The differences in calculated mixing-ratios between case C and D in Fig. 9 are very small and the form of the equation for the entrainment rate shows surprisingly no strong effect on the tracer redistribution. When we set E equal to zero (case B, Fig. 9), the shape function $f(z)$ equals 1 at all levels. In this case B, the mass transport in a single cloud has the same magnitude at all levels until the level ζ leading to stronger exchange from the ground to the middle troposphere and to lower transports into the upper troposphere compared to cases C and D.

As we have shown, the most sensitive parameters are the precipitation efficiency and the cloud height distribution. Generally, varying the parameters influences mainly the concentration in the upper troposphere and stronger the concentrations at ground. Most of the parameters in our scheme were first described by Austin and Houze (1973) who derived them from measurements in the tropics. Due to the lack of corresponding data at other latitudes, we will adopt basically the same parameter at other latitudes with the only difference that we choose other maximum cloud top heights. It is important to check our convection parameterization scheme with the aid of some observed tracers. In this study we use ^{222}Radon for this purpose.

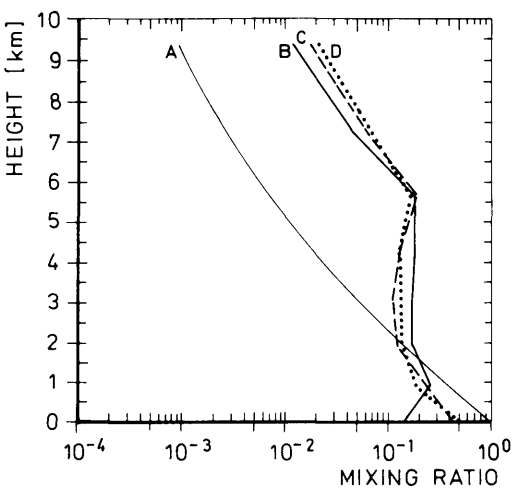

Fig. 9. Vertical profiles of the redistribution of the mass mixing-ratios of a tracer for varying the entrainment rates E. Curve A shows the initial tracer distribution, B the redistribution by one convective event with $E = 0$, C with $a = 0.2$ and D with $a = 0.5$ (see formula (12)).

6. Test of the convective scheme with ^{222}Rn and comparison with observations

The radioactive rare gas ^{222}Rn is a decay product of ^{238}U. It is the first gas in the uranium decay chain, and is mainly exhaled from land surfaces. As this process is the only source for ^{222}Rn and as its only sink is radioactive decay, it is a suitable tracer to test our model. Due to its half-life time of only 3.824 days the spatial, and especially vertical, distribution of radon shows great sensitivity to subgrid scale processes, such as deep convection.

From several studies (Turekian et al., 1977; Lambert et al., 1982; Dörr, 1984), emanation rates of ^{222}Rn were found to vary greatly depending on soil conditions and meteorological factors. It depends on the ^{226}Ra content of the soil and on soil porosity. Meteorological conditions such as strong precipitation and ice- or snow-cover leading to lower porosity and turbulent exchange in the boundary layer influence radon emanation rates. Observations during winter indicate a marked decrease when the soil is frozen (Pearson, 1965). Dörr (1984) reported a decrease of radon emanation to 30–40% of the normal flux when there is a snow-cover of 15 cm depth and no flux was observed from ice-covered ground. Transport of ^{222}Rn through plants due to the high concentration in soil gas is an effective mechanism to increase the exhalation rate. The flux of ^{222}Rn over mature corn fields may be 8 or 10 times larger than over bare soils (Martell, 1985). However higher emanation rates over agricultural land may partially also be caused by the use of phosphate fertilizer containing ^{226}Ra as reported by Dörr (1984), who measured a doubling

of radon emanation from intensively used agricultural soils.

Two principal methods are used to determine the flux of radon to the atmosphere. The first is the collection of ^{222}Rn emitted during a given time in a box covering the soil. The second is the integration of ^{222}Rn profiles in the atmosphere and the estimation of the flux assuming the balance between emanation and radioactive decay. Radon fluxes determined from direct measurements range from 0.004 atoms cm^{-2} s^{-1} in Wellington, New Zealand, to 2.5 atoms cm^{-2} s^{-1} in Champaign County, Illinois, USA (Turekian et al., 1977). Various studies have estimated the global average radon flux over land based on measurements to be 0.63 atoms cm^{-2} s^{-1} (Liu et al., 1984), 0.71 atoms cm^{-2} s^{-1} (Israel, 1958), 0.72 atoms cm^{-2} s^{-1} (Lambert et al., 1982) or 0.91 atoms cm^{-2} s^{-1} (Dörr, 1984). Turekian et al. (1977) from an extended survey argue that the true average radon flux probably exceeds these values and estimate the emanation flux with 1.2 atoms cm^{-2} s^{-1}. They pointed out that in the past most measurements have neglected the influence of transport through vegetation. In addition, the integrated atmospheric profile measurements yield the steady-state value only after the air mass has traversed a continent for several days, so that in several cases such measurements were likely substantially diluted by maritime air.

According to Dörr (1984) radon emanation from soils shows no pronounced seasonal variation and seasonality is only influenced by conditions such as ice-cover and soil wetness. However, seasonality of emissions may be caused by the vegetation cover. In this study we neglect, however, seasonality and assume a constant emanation flux, except when there is ice cover in the model. Snow cover reduces the Rn flux to 40% in the case of snow cover deeper than 15 cm (Dörr, 1984). The monthly snow cover climatology was taken from the ECMWF model. Otherwise, we adopt the flux of of 1.2 atoms cm^{-2} s^{-1} by Turekian et al. (1977) from land surfaces as a global average. We assume that the large grid-area of $10° \times 10°$ leads to smoothing of local differences. The emanation rate from the sea is 100 times less (Broecker et al., 1967) than from soils and is therefore neglected in this study.

Calculated global distributions of ^{222}Rn at the surface are shown in Fig. 10 for the months of January and July. Differences between the two months reflect the seasonality of transport as well as the lack of emission due to snow-cover in the northern winter hemisphere. The main feature of the distribution is the sea–land contrast corresponding to the dominance of continental sources and the short life-time of radon. The values over land range from 60–150 pCi m_{STP}^{-3} (1 pCi m_{STP}^{-3} $= 10^{-12}$ Curie m^{-3} at standard temperature and pressure), while values over the oceans are less than 10 pCi m_{STP}^{-3}. Lambert et al. (1982) estimated, based on observations, the gobal inventory of radon and found values between 70–170 pCi m_{STP}^{-3} (average 125 pCi m_{STP}^{-3}) at ice-free continental sites, 3–10 pCi m_{STP}^{-3} over the oceans in the northern hemisphere and 0.5–1.8 pCi m_{STP}^{-3} in the southern hemisphere. These estimations agree very well with our simulations with the only exception that the model overestimates the concentration over the southern hemispheric oceans by about 0.5 pCi m_{STP}^{-3}.

To demonstrate the influence of convective processes the radon distribution for January at the 500 hPa level is shown in Fig. 11 and compared to a simulation without convective transports. Upward transport in regions with high convective activity leads to much higher concentrations. Strong advection takes place in the middle troposphere and results in high concentrations distinctly visible in the summer hemisphere eastward of the continents at higher latitudes and westward at low latitudes due to the prevailing wind regimes.

Fig. 12 show the calculated zonally averaged radon mixing-ratio (upper graphs) as a function of latitude and altitude for January and July. The surface mixing-ratios are high at latitudes with high radon emission rates, i.e., at latitudes with high land areas and no snow cover. In the upper troposphere high mixing-ratios are found in the tropics and in summer at mid-latitudes where intense convective activity leads to rapid upward transport of radon. Vertical gradients vary with latitudes. They are small for latitudes with a small fraction of land cover but high for latitudes with high land cover and small vertical exchange. Here the mixing-ratios at 500 hPa are about 25% of the values at the surface in summer and only 5–10% in winter. Mixing-ratios at levels above 300 hPa are less than 5% of the surface values at any time. In regions with high convective

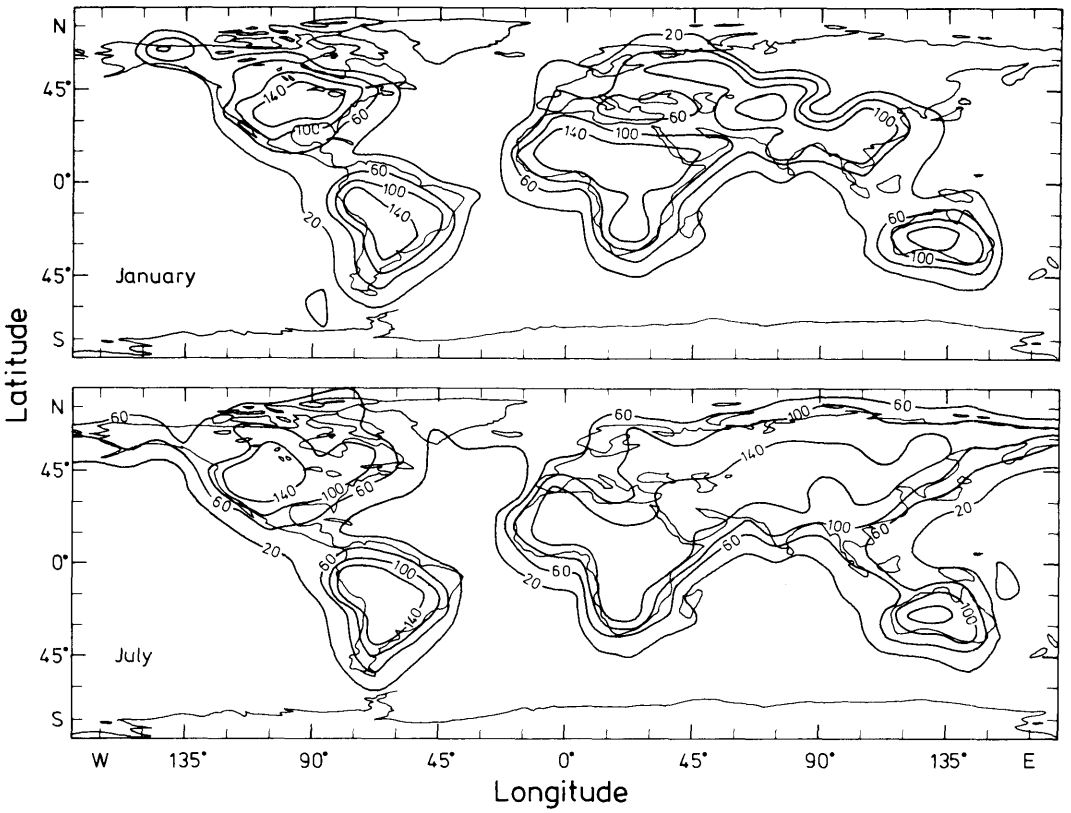

Fig. 10. Calculated global surface distribution of ^{222}Rn in pCi m_{STP}^{-3} for January and July.

activity, in the intertropical convergence zone, the middle atmosphere between 700 and 300 hPa is well-mixed, whereas the vertical gradients above 300 hPa and below 700 hPa are quite pronounced. The lower graphs of Fig. 12 depict the differences between model runs with and without convection.and show the change in the mixing-ratio caused by convective transport. Negative values denote a loss and positive values a gain of tracer by convective processes. The simulations reflect the existence of strongest vertical exchange in the tropics and at mid-latitudes in summer. Surprisingly, the convective mass transport in summer at mid-latitudes is only little less than in the tropics. This may be due to the fraction of convective rain of the total amount of precipitation, which was taken from the model output of the ECMWF. As shown in Fig. 2 this fraction which is 70–80% in the tropics is only slightly higher than the fraction of 70%, at northern mid-latitudes during summer.

As the MOGUNTIA model is driven by mean climatological conditions, the results of calculated tracer distributions must also be interpreted as climatological means. Unfortunately, there are only few measurements of radon that were taken continually over a sufficient time span to give representative seasonal means. Especially in the middle and higher troposphere the available data are scarce and the few vertical profiles are very variable depending on the special meteorological situation.

Continually surface measurements at Freiburg/FRG (47.9°N, 7.8°E) covering the period from 1982 to 1988 were performed by Weiss (1989). Monthly means are presented in Fig. 13 (solid line) and compared to model simulations. Low radon mixing-ratios during the spring reflect a

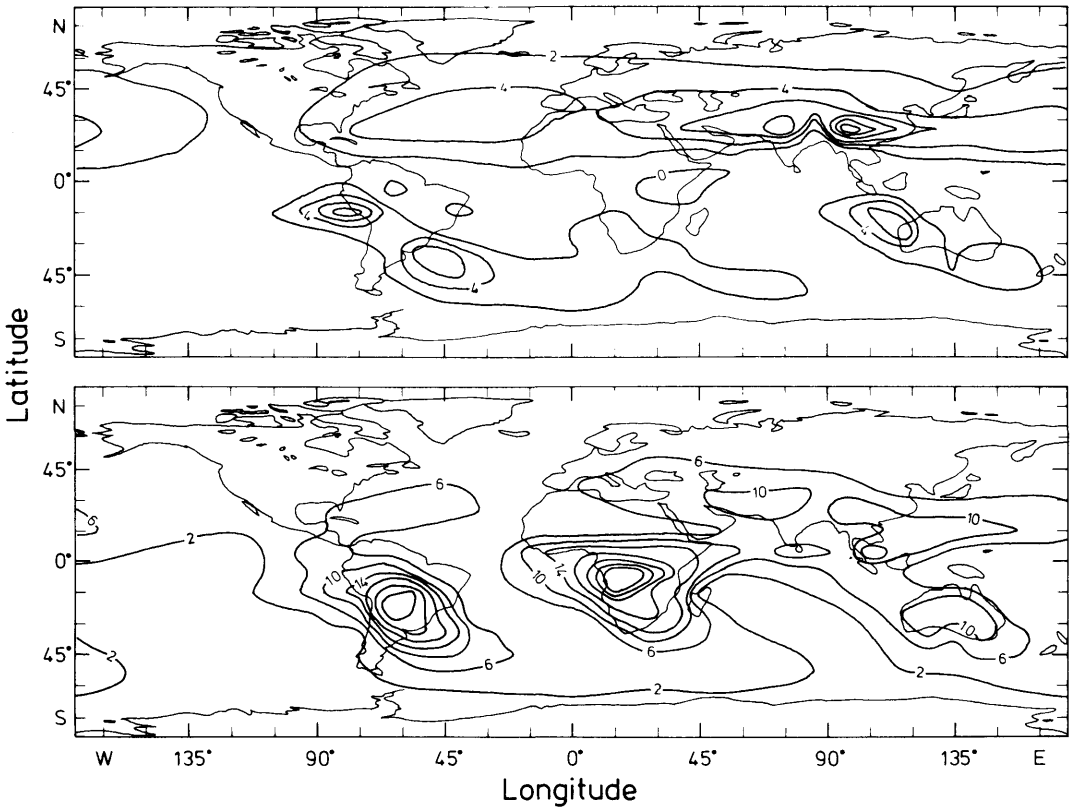

Fig. 11. Calculated global distribution of ^{222}Rn in pCi m_{STP}^{-3} at 500 hPa level for January; upper graph: no convective transport; lower graph: with convective transport.

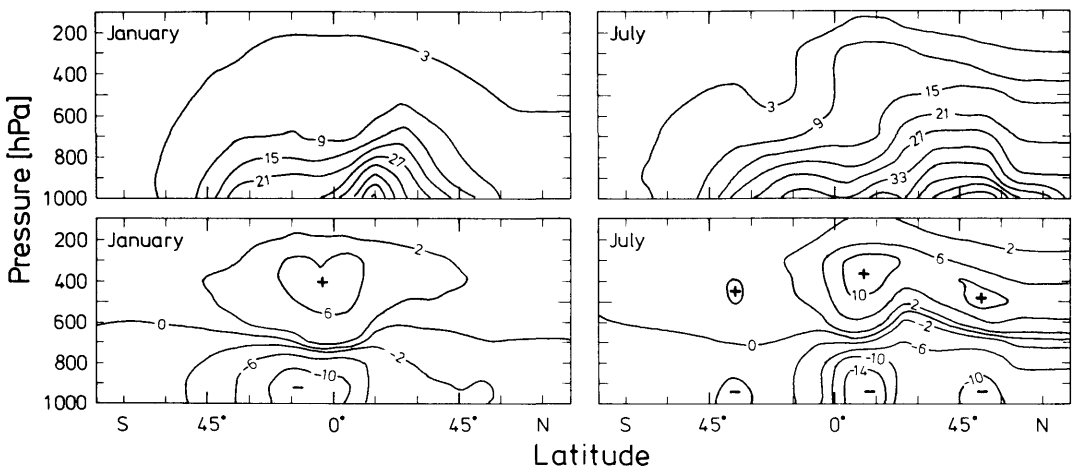

Fig. 12. Zonally averaged ^{222}Rn mixing-ratio in pCi m_{STP}^{-3} as a function of latitude and altitude for January and July; upper graph: model simulation with convective transport; lower graph: differences between model runs with and without convective transport.

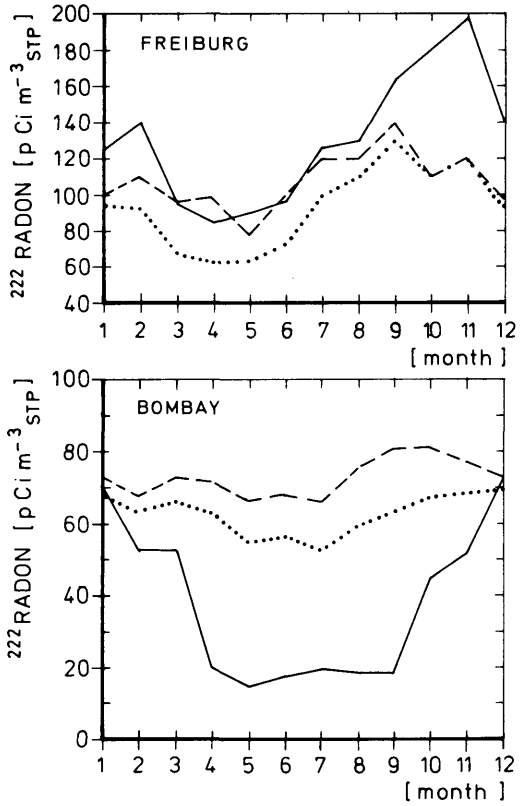

Fig. 13. Comparison of ^{222}Rn concentration at surface between observations (solid line) and model prediction with (dotted line) and without convective transport (dashed line) for Freiburg/FRG and Bombay/India.

stronger cyclonal activity whereas stable conditions in the boundary layer during the fall lead to higher radon values. The seasonality of observations and model simulations agrees quite well except during fall. The maximum value of the calculations is not as distinctly marked as the observed values and appears two months earlier. The simulated values are generally lower than the observed one as the lowest level does not represent the surface concentration but an average of the lowest 50 hPa. Differences between model runs with (dotted line) and without (dashed line) convective transport are strongest during spring and summer and vanish during the fall. The maximum difference in April amounts to 40%.

Gesell (1983) presents a survey of long-time surface radon observations most of them at mid-latitudes. For comparison with our model results we have chosen the station Bombay/India (18° N, 73° E) expecting a higher convective activity than in higher latitudes. The measurements cover a period of 10 years and were not taken all day but only during the afternoon. Observations (Fig. 13, solid line) show high radon values during the winter when continental radon enriched air is advected. With the advent of spring the wind regime changes to the familiar monsoon pattern and the advection of marine air reduces rapidly the radon mixing-ratios. The model seems not to be able to simulate this strong decrease and shows much too high values during spring and summer. These higher mixing-ratios may result from the coarse horizontal grid resolution, at which one grid point represents the whole Indian continent. Consideration of convective transport (dotted line) leads to lower radon mixing-ratios all over the year, especially during the fall when the convective activity under the influence of the high sea surface temperature is very strong.

Long time observations of vertical radon profiles, which are necessary to confirm vertical transport processes, do not exist. Consequently we had to use the sporadic measurements on radon that have been made so far and that may not represent mean meteorological conditions. Three vertical profiles, averages of several measurements, were chosen for comparison with model prediction (Fig. 14).

Liu et al. (1984) collected 23 published vertical profiles of radon from five locations in the USA and from two sites in the USSR measured in summer and calculated an average profile reaching up to 12 km (Fig. 14a, solid line). The dotted line denotes a simulation run with convection, the dashed line one without convective transport. Both model profiles represent averages of the summer months taken at the same sites as in Fig. 14a. The observed and the calculated profile agree very well; only near the surface the discrepancy amounts to about 30%. The neglect of convective processes would strongly underestimate mixing-ratios at altitudes above 4 km, leading to maximum differences of two orders of magnitude at 100 hPa.

A further comparison was made with measurements by Wilkening (1970) at New-Mexico (34° N, 106° W), USA, as depicted in Fig. 14b. It shows a mean profile averaged from six flights in

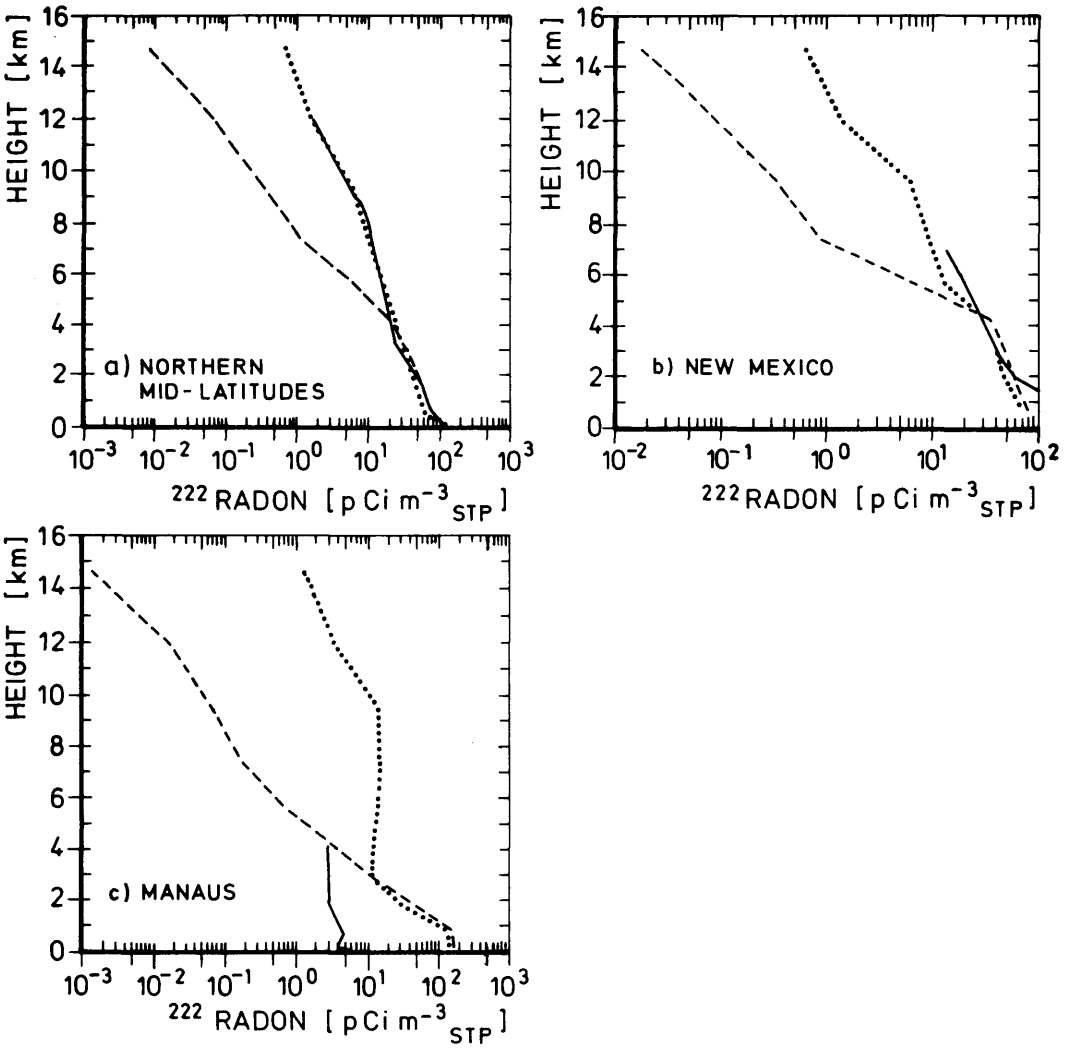

Fig. 14. Comparison between observed vertical 222 Rn profiles (solid line) and model prediction with (dotted line) and without convective transport (dashed line).

July up to 6 km altitude. The calculated values near the surface are again too low but in the middle troposphere model mixing-ratios deviate very little from the observations. The influence of convective transports is again distinctly marked above 4 km.

Fig. 14c shows an average of two profiles observed at Manaus (3°S, 60°W), Brazil, in April by Pereira et al. (1988). Their radon concentrations are surprisingly low when compared to measurements in other continental regions (<17 pCi m_{STP}^{-3} at ground and 3 pCi m_{STP}^{-3} at 4 km altitude). Calculated mixing-ratios, however, are 105 pCi m_{STP}^{-3} near the earth's surface and 10 pCi m_{STP}^{-3} at 4 km altitude. Pereira et al. (1988) estimated a radon flux of 0.33 atoms cm^{-2} s^{-1}, lower by a factor of four when compared to our model assumption. Intercomparison with our theoretical results indicates that average emission rates may be even lower than 0.33 atoms

$cm^{-2}\,s^{-1}$. As these measurements were made during the rainy season it seems likely that the emission of radon is strongly diminished when the soil is saturated with water. Moreover, the low mixing-ratios could be caused by dilution with maritime air. Due to the high convective activity in the wet season, measured and calculated profiles show a rather well mixed atmosphere above 2 km respectively 3 km in the simulation run, whereas the mixing-ratio decreases exponentially with height when convective transport is neglected. The strong gradient near the ground cannot be resolved by the model due to the coarse grid resolution but, however, the exchange in the lowest levels seems to be too weak.

7. Conclusions

The simulation of short-lived tracer distributions in a three-dimensional chemical tracer transport model requires the consideration of subgrid-scale processes, especially deep convection. Here we have developed a scheme for deep convection parameterization, based on the ideas proposed by Austin and Houze (1973), which we have tested with ^{222}Rn observations. The comparison between model predictions and measurements of ^{222}Radon with a half-life time of 3.8 days indicates that model runs without rapid upward draft in convective cells lead to mixing-ratios which in the upper troposphere in the tropics are up to four orders of magnitude lower than observations, whereas the parameterization of deep convection in general gives far better correspondence with measurements of radon mixing-ratios.

Unfortunately, radon observations exist only for non-tropical latitudes, whereas most of the convective activity takes place in the tropics. Radon as a chemical inert gas is an excellent tracer for testing transport parameterization in atmospheric modelling and it is therefore highly desirable to obtain many more radon observations from all around the world, especially from tropical regions.

Of course, ultimately, ^{222}Rn is only one of many possible tracers to study rapid vertical exchange processes in the troposphere. Its great advantage is its simple "chemistry" and rather well defined and homogeneous emission fluxes at the earth's surface. For many chemically reactive, important trace gases, the atmospheric lifetimes are of the order of hours to weeks, so that for those convective processes are likewise of the utmost importance to define their global distributions and chemical effects. Examples are reactive hydrocarbons (Greenberg and Zimmerman, 1984; Ehhalt et al., 1985), sulfur gases (Maroulis et al., 1980; Chatfield and Crutzen, 1984; Ockelmann, 1988) and NO_x (Kley et al., 1981).

8. Acknowledgements

This work was supported by the Ministry for Research and Technology of the Federal Republic of Germany through grant BMFT/KBF 68 and by the German Science Foundation (DFG) through grant SFB233/A4.

REFERENCES

Austin, P. M. and Houze, R. A. 1973. A technique for computing vertical transports by precipitating cumuli. *J. Atmos. Sci. 30*, 1100–1111.

Braham, R. R. 1952. The water and energy budgets of the thunderstorm and their relationship to thunderstorm development. *J. Meteorol. 9*, 227–242.

Broecker, W. S., Li, Y. H. and Cromwell, J. 1967. Radium 226 and Radon 222; concentration in Atlantic and Pacific oceans. *Science 158*, 1307–1310.

Chatfield R. B. and Crutzen, P. J. 1984. Sulfur dioxide in remote oceanic air: cloud transport of reactive precursors. *J. Geophys. Res. 89*, 7111–7132.

Cheng, C. P. and Houze, R. A. 1979. The distribution of convective and mesoscale precipitation in GATE radar echo patterns. *Mon. Wea. Rev. 107*, 1370–1381.

Covey, C., Thompson, S. L. and Schneider, S. H. 1985. Nuclear winter: a diagnosis of atmospheric general circulation model simulations. *J. Geophys. Res. 90*, 5615–5628.

Crutzen, P. J. and Gidel, L. T. 1983. A two-dimensional photochemical model of the atmosphere. *J. Geophys. Res. 88*, 6641–6661.

Delsol, F., Miyakoda, K. and Clarke, R. H. 1971. Parameterized processes in the surface boundary

layer of an atmospheric circulation model. *Quart. J. R. Meteorol. Soc. 97*, 181–208.

Dörr, H. 1984. Investigation of the gas and water budgets in the unsaturated soil layer using carbondioxid and radon 222 (in German). Ph.D. thesis, Universität Heidelberg, FRG.

Dümenil, L. and Schlese, U. 1987. Description of the general circulation model. In: *Climate simulation with the ECMWF T21-model in Hamburg* (ed. G. Fischer). Rep. Nr. 1, Meteorologisches Institut, University of Hamburg, FRG, 3–9.

Ehhalt, D. H., Rudolph, J., Meixner, F. and Schmidt, U. 1985. Measurements of selected C_2–C_5 hydrocarbons in the background troposphere: vertical and latitudinal variations. *J. Atmos. Chem. 3*, 29–52.

Frank, W. M. and Cohen, C. 1985. Properties of cloud ensembles estimated using a cloud model and an observed updraft population. *J. Atmos. Sci. 42*, 1911–1928.

Gesell, T. F. 1983. Background atmospheric ^{222}Rn concentrations outdoors and indoors: A review. *Health Physics 45*, 289–302.

GFDL Atmospheric Circulation Tape Library, 1958–1973. National Climatic Data Center, Ashville, NC, USA.

Gidel, L. 1983. Cumulus transport of transient tracers. *J. Geophys. Res. 88*, 6587–6594.

Green, J. S. A. 1970. Transfer properties of the large-scale eddies and the general circulation of the atmosphere. *Quart. J. R. Meteorol. Soc. 96*, 157–185.

Greenberg, J. P. and Zimmerman, P. R. 1984. Nonmethane hydrocarbons in remote tropical, continental, and marine atmospheres. *J. Geophys. Res. 89*, 4767–4778.

Hahn, C. J., Warren, S. G. London, J., Chervin, R. M. and Jenne, R. 1982. Atlas of simultaneous occurrence of different cloud types over the ocean. NCAR/TN-201+STR, National Center for Atmospheric Research, Boulder, Colorado, USA.

Houze, R. A. and Leary, C. A. 1976. Comparison of convective mass and heat transports in tropical easterly waves computed by two methods. *J. Atmos. Sci. 33*, 424–429.

Israel, H. 1958. The natural radioactivity in soil, water and atmosphere (in German). *Beitr. zur Physik d. Atmos. 30*, 177–188.

Jaeger, L. 1976. The distribution of global monthly means of precipitation (in German). *Berichte des Dt. Wetterdienstes 139*.

Kao, S. K. 1974. Basic characteristics of global scale diffusion in the troposphere. *Advances in Geophysics 18B*, 15–32.

Kley, D., Drummont, J. W., McFarland, M. and Liu, S. C. 1981. Tropospheric profiles of NO_x. *J. Geophys. Res. 86*, 3153–3161.

Lambert, G., Polian, G., Sanak, J., Ardouin, B., Buisson, A., Jegou, A. and Le Roulley, J. C. 1982. The cycle of radon and its decay products: An application to the study of tropospheric–stratospheric exchange (in French). *Ann. Géophys. 38*, 497–531.

Liu, S. C., McAffee, J. R. and Cicerone, R. J. 1984. Radon-222 and tropospheric vertical transport. *J. Geophys. Res. 89*, 7291–7297.

Mahlmann, J. D. and Moxim, W. J. 1978. Tracer simulation using a global general circulation model: Results from a mid-latitude instantaneous source experiment. *J. Atmos. Sci. 35*, 1340–1378.

Malone, R. C., Auer, L. H., Glatzmaier, G. A., Wood, M. C. and Toon, O. B. 1986. Nuclear winter: Three-dimensional simulations including interactive transport, scavenging, and solar heating of smoke. *J. Geophys. Res. 91*, 1039–1053.

Maroulis, P. J., Torres, A. L., Goldberg, A. B. and Bandy, A. R. 1980. Atmospheric SO_2 measurements on project Gametag. *J. Geophys. Res. 85C*, 7345.

Martell, E. A. 1985. Enhanced ion production in convective storms by transpired radon isotopes and their decay products. *J. Geophys. Res. 90*, 5909–5915.

Murgatroyd, R. J. 1969. Estimation from geostrophic trajectories of horizontal diffusivity in the mid-latitude troposphere and lower stratosphere. *Quart. J. R. Meteorol. Soc. 95*, 40–62.

Newell, R. E., Kidson, J. W., Vincent, D. G. and Boer, G. J. 1972. The general circulation of the tropical atmosphere, Vol. I, II. Cambridge, Mass.

Ockelmann, G. 1988. Large-scale distribution of atmospheric sulphurdioxyde in the troposphere and lower stratosphere—results of an experimental study (in German). Berichte des Instituts für Meteorologie und Geophysik der Universität Frankfurt/Main, FRG, Nr. 75.

Oort, A. H. 1983. Global atmospheric circulation statistics, 1958–1973. NOAA professional paper No. 14, U.S. Government Printing Office, Washington, DC.

Pasquill, F. 1974. Limitations and prospects in the estimation of dispersion of pollution on a regional scale. *Advances in Geophysics 18B*, 1-13.

Pearson, J. E. 1965. Radon-222, A study of its emanation from soil, source strength, and use as a tracer. Research Reports, Dept. of General Engineering, Univ. of Illinois, Urbana, USA.

Pereira, E. B., Nordemann, D. J. R. ,Wofsy, S. C. and Trumbore, S. 1988. Vertical radon concentration profiles over the Brazilian Amazon basin during the wet season. *Eos 69*, No. 16.

Prather, M., McElroy, M., Wofsy, S., Russell, G. and Rind, D. 1987. Chemistry of the global troposphere: Fluorocarbons as tracers of air motion. *J. Geophys. Res. 92*, 6579–6613.

Ruprecht, E. 1982. An investigation of the tropical cloud clusters over the GATE area. Part II: Vertical transport by cumulus and cumulonimbus drafts and energy budgets. *Beitr. Phys. Atmosph. 55*, 85–107.

Turekian, K. K., Nozaki, Y. and Benninger, L. K. 1977. Geochemistry of atmospheric radon and radon products. *Ann. Rev. Earth Planet. Sci. 5*, 227–255.

Warren, S. G., Hahn, C. J., London, J., Chervin, R. M. and Jenne, R. L. 1986. Global distribution of total cloud cover and cloud type amounts over land. NCAR/TN-273+STR, National Center for Atmospheric Research, Boulder, Colorado, USA.

Weiss, W. 1989. Bundesamt für Zivilschutz, Institute for Atmospheric Radioactivity, Freiburg, FRG (personal communication).

Wilkening, M. H. 1970. Radon 222 concentrations in the convective patterns of a mountain environment. *J. Geophys. Res. 75*, 1733–1740.

Zimmermann, P. H. 1984. A three-dimensional numerical model for the transport of atmospheric tracers (in German). Ph.D. thesis, Universität Mainz, FRG.

Zimmermann, P. H. 1987. MOGUNTIA: A handy global tracer model. In: *Air pollution modeling and its application.* Proc. 16th NATO/CCMS Int. Tech. Mtg. Lindau, FRG, 6–10 April 1987, 593–608.

Zimmermann, P. H., Feichter, J., Rath, H. K., Crutzen, P. J. and Weiss, W. 1989. A global three-dimensional source-receptor model investigation using ^{85}Kr. *Atmos. Environment 23*, 25–35.